Vaporization of bi-component droplets in a turbulent over-heated flow : Experiments and Numerical Simulation

F. Moreau[2,3], G. Castanet[1], R. Bazile[2,3], F. Lemoine*[1]
*1: LEMTA, Nancy-Université, CNRS, Vandoeuvre-Lès-Nancy, France
2: Université de Toulouse ; INPT, UPS ; IMFT (Institut de Mécanique des Fluides de Toulouse) ; Allée Camille Soula, F-31400 Toulouse, France
3: CNRS ; IMFT ; F-31400 Toulouse, France

Abstract

This paper deals with an experimental study of bi-component droplets evaporation in a turbulent over-heated channel flow. Droplets are made of a mixture of n-octane and 3-pentanone (15% in volume). Planar Laser Induced Fluorescence (PLIF) of 3-pentanone is used to derive both concentration of this molecule in liquid and gas phases. Concomitant dispersion of the liquid droplets and evaporation can be clearly observed with a trend to homogenisation of the 3-pentanone vapour in the flowfield due to high turbulence rate, on the order of 40%.
The experimental results, in term of concentration of 3-pentanone in both liquid and gas phases have been compared to a simplified numerical simulation based on the discrete component model, taking into account the droplet composition, associated to the isolated droplet model. It appears that the measurements performed on the liquid phase overestimate the calculated evaporation, as the gas phase measurements performed far from the injection point are in correct agreement with the calculations. One of the explanations is that the PLIF CCD camera dynamic is not sufficient to detect simultaneously the biggest and smallest droplets. In the present cases, most of the numerous smallest droplets seem to be ignored by the measurement, which tends to overestimate the droplet evaporation. The second important cause of discrepancy between experimental and numerical results is linked to the strong extinction of the fluorescence signal issuing from the liquid phase, due to the absorption

---

Introduction

The fine understanding of droplet evaporation in a turbulent flow [1] is a fundamental issue connected with major applicative fields such as injection of liquid fuel in the combustion chamber of internal combustion engines. Development of advanced physical models taking into account dispersion of the fuel droplets by turbulence, evaporation, mixture of the fuel vapour in the gas phase, and connected predictive simulation tools will contribute to fuel consumption reduction and pollution abatement. The effect of turbulence on droplet evaporation seems to have contradictory effects. On the one hand, Birouk et al. [2] showed that turbulence increases isolated droplet evaporation rate. On the other hand, the formation of droplet clusters, because of turbulence, may locally increase the amount of vapour up to saturation and slow down the local evaporation [3]. In order to understand the evaporation of a spray in a turbulent flow, experimental data are needed. The case of high turbulence levels close to what is encountered in a real combustion chamber is studied here.

In the present study, a fuel spray made of a mixture of n-octane and 3-pentanone (15% in volume) is injected in an isotropic and homogeneous turbulent overheated flowfield. Measurements are carried out on liquid and gas phases (velocities, turbulence characteristics, droplet size distribution) with a special focus on liquid and gas 3-pentanone concentrations, which are derived from Planar Laser-Induced Fluorescence (PLIF) measurements on this molecule. Finally the experimental results in term of liquid and gas mass flowrate concentration will be compared to a simplified numerical simulation, which does takes into account the effect of turbulence and droplets collisions onto walls. The discrete component model, taking into account the droplet composition [4], associated to the isolated droplet model [5] will be used for each of the size classes in order to calculate the evaporated 3-pentanone flowrate. Agreement between experiments and calculation will be discussed in the light of the bias induced by PLIF measurements.

Experimental set-up, measurement techniques and results

- ***Experimental set-up***

The experimental set-up consists in a vertical square air tunnel (0.8 m length, 0.092 m large) where a high turbulence rate can be generated by a specially designed turbulence generator, initially developed by Videto and Santavicca [6]. Pressurized air is injected in a cylindrical enclosure (Fig. 1). The air is then forced through the bottom of the cylindrical chamber, pierced by 45 holes, each being 3 mm in diameter. The jets issuing from the 45 holes impact a convergent nozzle, directly linked to the square test section. With such a device, the turbulence intensity can reach 40% with a good isotropy in the major part of the flow field [7].

* Corresponding author: fabrice.lemoine@ensem.inpl-nancy.fr

The channel, which has a square shaped cross section (92x92 mm^2) is composed of four 160 mm long segments and one optical segment. The optical segment is 200 mm long and equipped with two small quartz windows (100 x 10 mm^2) and two large Pyrex windows (110 x 82 mm^2) allowing optical measurements all along the channel. The z axis is the longitudinal axis, starting from the entrance of the channel. The x axis is the radial axis. Their origins are taken at the centre of the square shaped cross section at the entrance of the channel. In the following sections, most results will be given versus z/H or y/H, where H = 92 mm is the width of the channel cross section. The injected liquid is a mixture of 3-pentanone (15 %) and n-octane (85 %).
The air can be pre-heated up to 423 K by means of a heater and the bulk velocity is 2 m/s. In order to create the droplet mist, an ultrasonic injector, cooled by a temperature regulated water flow, is placed at the centre of the channel, the tip of the nozzle being located at z/H=0. With this kind of atomizer the liquid flow is disintegrated using ultrasounds allowing small initial velocity for the droplets, on the order to 1.6 m/s whatever the size class is. The droplets sizes range from very small size neighbouring a few microns to 270 μm (Fig. 2).

Table 1- Experimental flow and spray conditions.

Temperature of the air	423 K
Bulk velocity	2m/s
Air mass flux	14.3 gr/s
Liquid mass flux	0.322 g/s
Volume fraction of 3-pentanone in the liquid mixing	15%
Temperature incoming liquid	293 K
Droplet mass fraction	2.2 %
Droplet volume fraction	2.5 10^{-5}

- ***PLIF experiments***

The velocity statistics of the continuous phase are measured by Laser Doppler Anemometry (LDA). The velocity and diameter of the droplets are measured using Phase Doppler Anemometry (PDA).
The evolution of the mean longitudinal velocity of the droplets is presented in figure 3. Except at the first stage after the injection zone ($< z/H = 0.6$), the droplets linked to the smallest size class follow the air flow. However, the droplets linked to the biggest size class, increase their velocities up to the terminal velocity. Intermediate behaviours are found for the droplets of intermediate size classes.

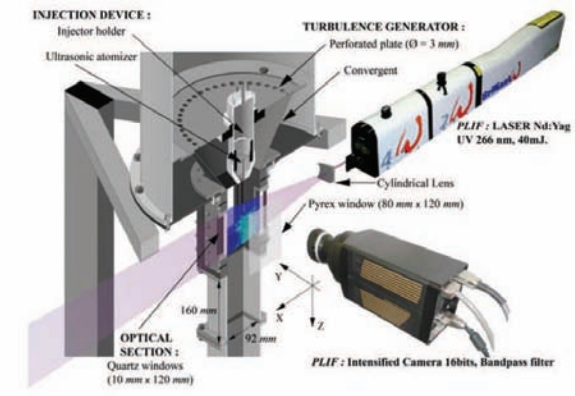

Figure 1. Experimental set-up.

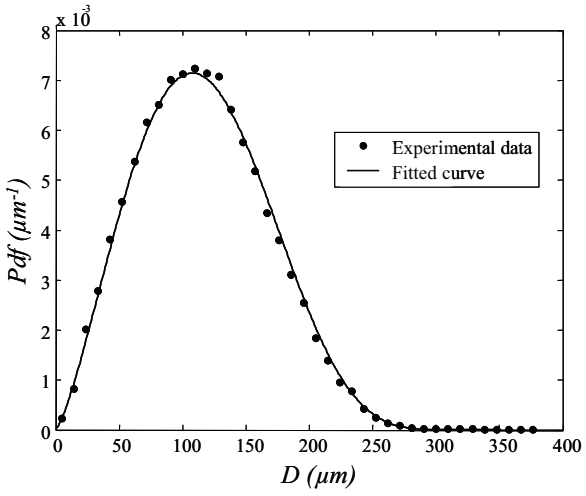

Figure 2. PDF of the droplet sizes at z/H=0.5 and T_{air}=423 K.

Planar Laser-Induced Fluorescence (PLIF) of 3-pentanone, induced by the quadrupled Nd:YAG laser (λ=266 nm) was used to determine the concentration of 3-pentanone in both liquid and vapour phases. The LIF technique is based on the physical phenomenon of fluorescence. When the fluorescent molecules are excited by a laser beam at a wavelength λ tuned on the fluorescent molecules absorption spectrum, a fluorescence signal, S, is emitted over a range of higher wavelength than the excitation light, thus allowing discrimination between

excitation and emission signals. Since the number of emitted photons is proportional to the number of excited molecules N, a direct measurement of the fluorescing molecules concentration is
The fluorescent molecule used in this study is 3-pentanone. Its photo-physical properties have been widely studied ([8] and [9]) for the vapour phase. The absorption spectrum of 3-pentanone in the UV extends from 230 to 340 nm with a peak at 285.5 nm for a range of temperatures between 298 and 423 K. The 3-pentanone fluorescence signal is emitted between 350 and 550 nm with a maximum at 420 nm. As these two spectra do not superimpose there is no fluorescence trapping.
According to Koch and Hanson [8], between 298 K and 423 K, the influence of the temperature on the signal of fluorescence per molecule, under nitrogen, is small, less than 5 %. According to Orain et al. [10] the influence of quenching by oxygen over this range of temperature is negligible. If the influence of the temperature is neglected, the fluorescence signal can be written with the following simplified expression:

$$S(x,\lambda,N) = I_0 N \sigma \Phi(\lambda,N) e^{-\sigma \int N(x) dx}$$

where x represents the position of the probe volume in the optical axis of the laser beam, σ is absorbing cross section at laser wavelength λ, I_0 is the incident laser intensity and Φ is the fluorescence quantum yield.
The only remaining bias is the dependency of the signal in the optical path from the entrance of the laser beam into the channel to the measurement point (along x), due to absorption by 3-pentanone molecules of the incident laser beam. This absorption of the laser is corrected along each radial line of the x axis. Then, the fluorescence signal can be written in a discrete way:

$$S(x,N) = I_0 N \sigma \Phi e^{-\sigma \sum_0^x N(x) \Delta x}$$

where Δx is the distance increment between two consecutive measurements.
The initial condition is taken at the entrance of the laser in the channel (x=0). Then, the pixel to pixel absorption correction can be used to derive the number of fluorescing molecules in the gas phase, which is directly linked to the 3-pentanone local concentration if the measurement volume is constant:

$$N(x) = \frac{S(x,N)}{S(0,N(0))} N(0) e^{\sigma \sum_0^x N(x) \Delta x}$$

Concerning the fluorescence of the liquid phase, no absorption effect is measured due to the presence of the droplets, due to the small volume fraction of the dispersed phase, on the order of 10^{-5}. It simply means that measurements performed in the gas phase are negligibly influenced by the liquid droplets absorption. The laser used for LIF experiments is a pulsed Nd:YAG laser, with the following characteristics: λ = 266 nm, energy = 30 mJ, repetition frequency 10 Hz. A vertical laser sheet is generated with a thickness of about 400 µm. The fluorescence signal is collected with a 16 bit, 1024 x 1024 pixels intensified camera (PIMAX-Princeton) and a 58 mm objective lens. A 300-500 nm band-pass filter is used to remove laser Mie scattering due to the presence of the droplets.
One of the main problems is to discriminate the liquid and vapour phase on instantaneous LIF images. The applied discrimination is based on median filtering (using a 7x7 structuring element). The filtered image is subtracted from the input image. The result is an image containing the high spatial frequencies. After morphological treatments of threshold, dilatation and erosion, a binary image is obtained. This binary image is applied to the input image. An image containing the vapour phase and another one containing the liquid phase is finally obtained (Fig. 4) [11].

- ***PLIF results***

Radial profiles of the mean concentration of 3-pentanone in the liquid phase are presented in figure 5, for different downstream positions. At the entrance of the channel (z/H = 0.60) most of the liquid is located on the centerline of the channel due to the central position of injection device. The peak enlarges and decreases downstream due to both dispersion of the droplets by turbulent structures of the flow and phase change. Assuming axi-symmetry of the droplet cloud, the liquid 3-pentanone mass flowrate corresponding to a given cross-section can be derived by (Fig. 6):

$$\dot{m}_{3p} = 2\pi \int_0^{H/2} \overline{C_l}(r) \overline{W}_{vol}(r) r dr \quad \text{where } \overline{W}_{vol}(r) = \sum_{j=1}^{n} W_j D_j^3 \Big/ \sum_{j=1}^{n} D_j^3$$

where $\overline{C}_l$ denotes the 3-pentanone mean liquid concentration, j is the PDA sampling index and n is the number of samples detected by the PDA.

The mean droplet velocity $\overline{W}_{vol}(r)$ is calculated by weighing the velocity determined by the PDA for each droplet diameter by D^3, due to the fact that the mass of a droplet is proportional to D^3.

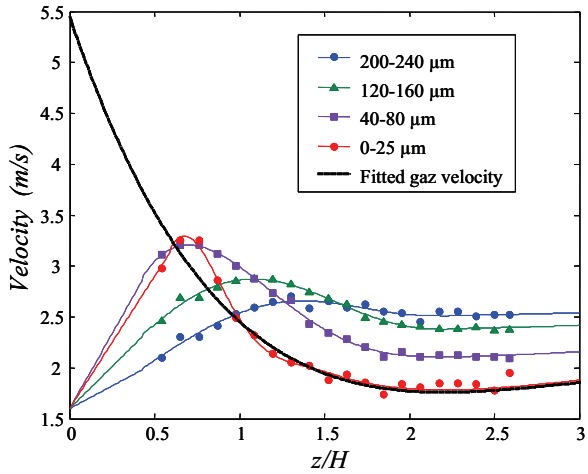

Figure 3. Axial evolution of normalized mean longitudinal velocity, at $x = y = 0$, for air (solid line) and droplets per size class (dots: measurements, lines: fitted curves used for the simulations).

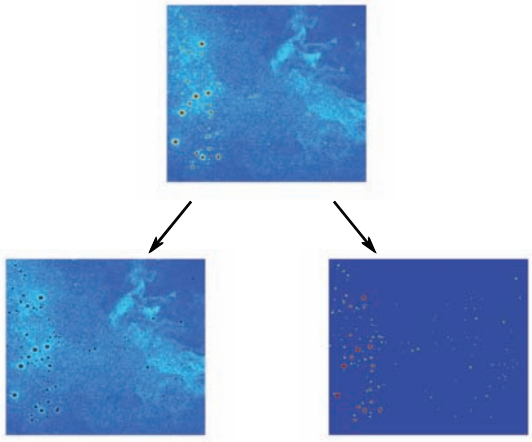

Figure 4. Liquid-vapour phase discrimination.

The radial profiles of the mean concentration of 3-pentanone in the vapour phase (Fig. 7) are flat from z/H = 3.14. The small dissymmetry can be explained by an imperfect correction of the absorption of the laser beam. The 3-pentanone mass flowrate in the vapour phase is obtained in each cross-section by integrating the concentration profiles using the bulk velocity (Fig. 8). The value 1 of the normalized mass flowrate (normalization is performed by the injected mass flowrate) corresponds to the total vaporization of the liquid phase. The observed value corresponds to 93% of the injected flow-rate, which means that not all the droplets are vaporised at z/H=5.

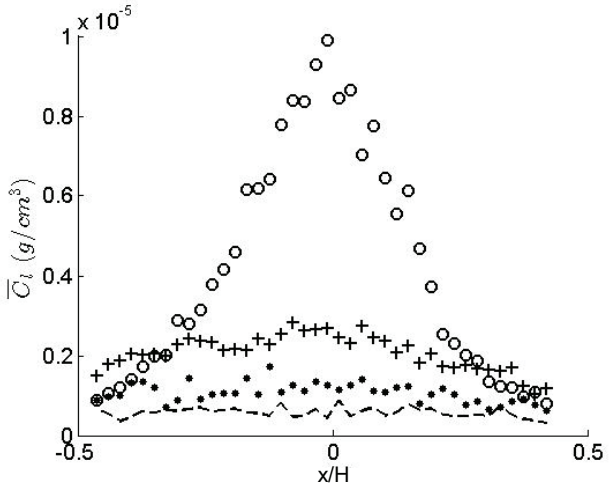

Figure 5. Radial profiles of the mean concentration of 3-pentanone in the liquid phase at z/H = 0.60 (o), z/H = 1.03 (+), z/H = 1.52 (•), z/H = 1.96 (-).

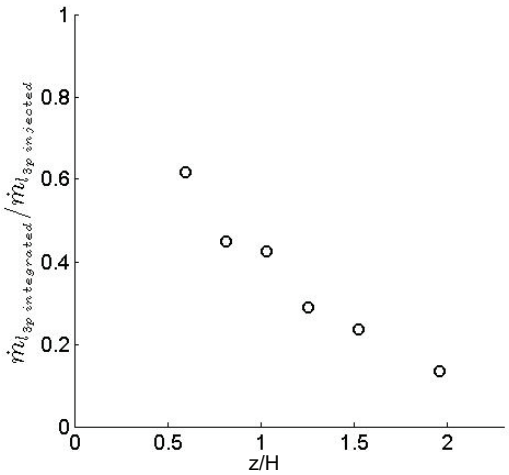

Figure 6. Axial evolution of the 3-pentanone mass flowrate in the liquid phase.

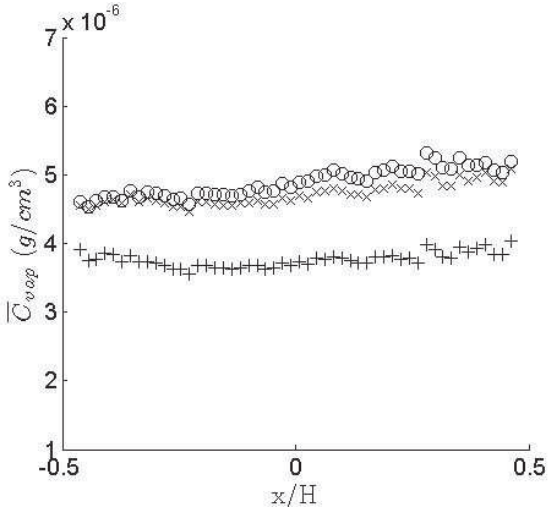

Figure 7. Radial profiles of the mean concentration of 3-pentanone in the vapour phase at z/H = 3.14 (+), z/H = 4.08 (X), z/H = 4.88 (o).

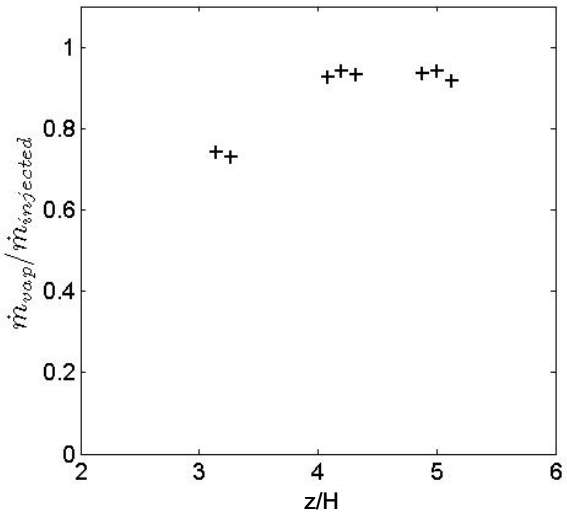

Figure 8. Axial evolution of the 3-pentanone mass flow-rate in the gas phase**.**

Numerical simulations

The experimental results were compared with a simplified model of droplet evaporation. This model considers that the heat and mass transfers inside the droplets results from pure diffusion and advection by the internal motions due to the friction between the liquid droplet surface and the external air flow. The evolution of the liquid composition is described by the discrete components approach presented by Tong and Sirignano [12], which consists in following each chemical species individually. Denoting $\xi = r/r_d(t)$, the equation for mass and heat transports within a droplet can be presented in the following form:

$$\frac{\partial Z}{\partial t} + \beta\,\xi\,\frac{\partial Z}{\partial \xi} = D_{eff}\left(\frac{\partial^2 Z}{\partial \xi^2} + \frac{2}{\xi}\frac{\partial Z}{\partial \xi}\right), \text{ with } \beta = \frac{\dot{r}_d}{r_d}$$

In this equation, Z corresponds to the temperature T or the mass fraction $Y_{l,i}$ *of* the i^{th} species in the mixture. D_{eff} is either the thermal effective conductivity or the liquid mass effective diffusivity of specie i into the liquid mixture. Abramzon and Sirignano [5] introduced the concept of effective diffusivity in the case of the sole heat transfer. This concept can be extended to the liquid mass transfer. Equation is solved in the absence of the convective term but the diffusion coefficient D_l (either the mass diffusivity $D_{l,i}$ or the thermal diffusivity $a_l=\lambda_l/\rho_l\,Cp_l$) is increased by a factor χ ranging from 1 to 2.72 to account for the effect of the internal circulation:

$$D_{eff} = \chi\, D_l\,,$$

where χ is a function of the thermal or the mass Peclet number Pe given in [5]. For the resolution, equation is supplemented by the following boundary conditions:

$$\lambda_l \left.\frac{\partial T}{\partial r}\right|_{r=r_d-0} = 2\pi\,\lambda_g\, r_d\, Nu\left(T_\infty - T_S\right) - \sum_i L_{v,i}\dot{m}_i\,,$$

$$\dot{m} = 2\,\pi\,\rho_g\, r_d\, D_{v,\mathrm{i}}\, B_{M,i} Sh_i\,,$$

where Nu and Sh_i are respectively the Nusselt and the Sherwood numbers. $D_{v,i}$ is the diffusion coefficient of specie i in air and $B_{M,i} = \dfrac{Y_{vs,i} - Y_{v\infty,i}}{\varepsilon_i - Y_{vs,i}}$ is the mass transfer Spalding number corresponding to the specie i. In the present calculations, the ambient temperature T_∞ is fixed at 423 K and $Y_{v\infty,\mathrm{i}}$ is assumed to be equal to 0. This approximation is justified by the fact that the mass flowrates of 3-pentanone and n-octane are very small in comparison to the mass flow rate of air crossing the channel. Assuming $Y_{v\infty,\mathrm{i}}$=0, the value of ε_i can be found easily by the following relation :

$$\varepsilon_i = Y_{vs,i} \Big/ \sum_i Y_{vs,i}\,.$$

The initial condition for the calculations corresponds to an uniform temperature and mass fraction in the droplet: $Y_{l,3\text{-}p}(t=0)=16\%$ and $T_l(t=0)=298$ K. The evaporation is described within the frame of the quasi-steady approach and the film theory [5]. Nusselt and Sherwood numbers are then given by :

$$Nu = 2\frac{\ln\left(1+B_T\right)}{B_T}\left[1+\frac{\left(1+Re\,Pr\right)^{1/3}\max\left(1,Re^{0.077}\right)-1}{2F\left(B_T\right)}\right]$$

$$Sh_i = 2\frac{\ln\left(1+B_{M,i}\right)}{B_{M,i}}\left[1+\frac{\left(1+Re\,Sc_i\right)^{1/3}\max\left(1,Re^{0.077}\right)-1}{2F\left(B_{M,i}\right)}\right]$$

where $F\left(B\right)=\left(1+B\right)^{0.7}\frac{\ln\left(1+B\right)}{B}$ and $B_T=\frac{\left(\sum_i \dot{m}_i Cp_{v,i}\right)\left(T_\infty-T_S\right)}{\left(\sum_i \dot{m}_i\,Lv_i\right)+Q_L}$ is the heat transfer Spalding number. B_T and $B_{M,i}$ are linked by the following equation :

$$B_T=\left(1+B_{M,i}\right)^{\varphi_i}-1$$

where $\varphi_i=\frac{Cp_{v,i}}{Cp_{air}}\frac{1}{Le_i}$ and $Le_i=\lambda_g/\rho_g\,Cp_g D_{v,i}$ is the Lewis number. The composition of the vapor near the droplet surface is assumed to be in equilibrium with the liquid mixture. In addition the liquid and vapor mixtures are considered to be ideal so that the Raoult law can be applied:

$$x_{sv,i}P_a = x_{sl,i}P_{sat,i}\left(T_S\right)$$

where x denotes the molar fraction. P_a=1atm is the ambient pressure in the channel, T_s is the droplet surface temperature and P_{sat} is the saturating vapour pressure.

To solve equation , the droplet is divided into 100 regular segments along the radial coordinate and a Crank-Nicholson scheme is used. At each time step, the droplet radius is updated to account for the loss of mass and the swelling. Downstream distance from the injector is converted into time with the help of the space evolution of the droplet velocity measured using the PDA technique. Figure 3 shows the evolution of the droplet average axial velocity for different size classes. As expected, the smallest droplets have a relative velocity almost equal to 0. These droplets follow the free stream. In the absence of measurements near the injector, it is assumed that the initial velocity of the droplets is independent of their size, this behaviour being generally observed for ultrasonic injectors. The axial velocity is also used to calculate the Reynolds number in equations and .

$$Re=\rho_{air}\left|V_d-V_g\right|D/\mu_g$$

The effect of turbulence on evaporation at any scale is not taken into account in the simulations, which are also reduced to a single dimension domain. In particular, the influence of the channel wall is ignored. In figure 4, it is also apparent that the mean liquid concentration is not uniform in a section of the channel near the injection but it tends to become uniform rapidly after.

The calculations were performed for a large number of droplet sizes ranging from 1 µm to 300 µm (maximum size observed by the PDA at z/H=0.6). The pdf of the droplet sizes obtained experimentally at z/H = 0.6 is interpolated as shown in figure 2. The fitted pdf is then used to determine the number of droplets to be considered to have a mass liquid flow rate of 3-pentanone comparable with the measurement at z/H = 0.6. Denoting N the number of droplet crossing a channel section per unit of time:

$$N\left(z/H=0.6\right)=\frac{\dot{m}_{l,3-p}\left(z/H=0.6\right)}{\int_0^\infty \rho_l\left(D\right)\frac{\pi D^3}{6}Y_{l,3-P}\left(D\right)P_{z/H=0.6}\left(D\right)dD}$$

where $P_{z/H=0.6}\left(D\right)$ is the size pdf at z/H=0.6. N decreases with z due to the disappearance of the droplets that have evaporated completely before reaching z. N is evaluated for any distance z as followed:

$$N(z) = N(z/H = 0.6) \int_{D_{min}}^{\infty} P_{z/H=0.6}(D)\,dD$$

where D_{min} is the minimum size in $z/H = 0.6$ for a droplet to be present downstream in the z section despite of the evaporation. The size PDF is calculated as follows:

$$P_z(D) = \frac{P_{z/H=0.6}(D_1)}{\int_{D_{min}}^{\infty} P_{z/H=0.6}(D)\,dD}$$

In this expression, a droplet having a size D in the z section has a diameter D_1 when it was in $z/H = 0.6$. Finally the liquid mass flow rate of 3-pentanone is evaluated using the following equation:

$$\dot{m}_{l,3-p}(z) = N(z) \int_0^{\infty} \rho_l(D) \frac{\pi D^3}{6} Y_{l,3-P}(D) P_z(D)\,dD$$

where $Y_{l,3\text{-}p}(D)$ and $\rho_l(D)$ corresponds to the results of the simulation obtained for a droplet of size D at the distance z.

The mass flow-rate of the 3-pentanone ($\dot{m}_{g,3-p}$) in the gas phase can be derived by:

$$\dot{m}_{g,3-p}(z) = \dot{m}_{l,3-p}(z=0) - \dot{m}_{l,3-p}(z)$$

Results and discussion

The computed droplet diameter evolution as a function of the downstream position is represented in figure 9 for different initial droplet diameters, in parallel with3-pentanone mass fractions (Y_{3P}) evolution (Fig. 10). The total evaporation of the droplets is observed at about z/H=1 for droplet diameters less than 50 µm. It is also noticed that a very fast depletion of the 3-pentanone occurs for the smallest droplets, as this depletion appears slower for the biggest one.

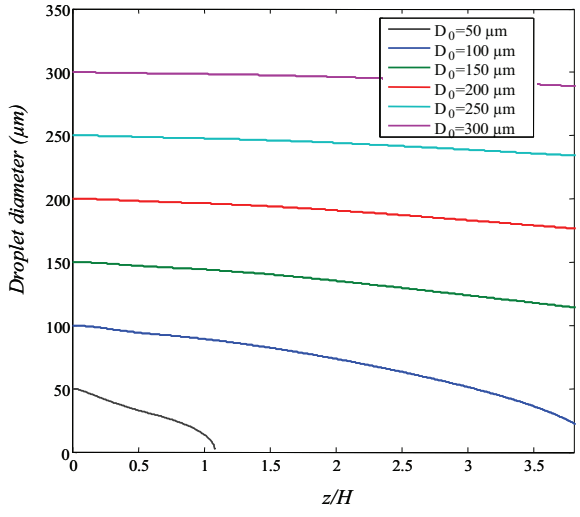

Figure 9. Computed droplet diameter evolution as a function of the downstream position for different initial droplet diameter.

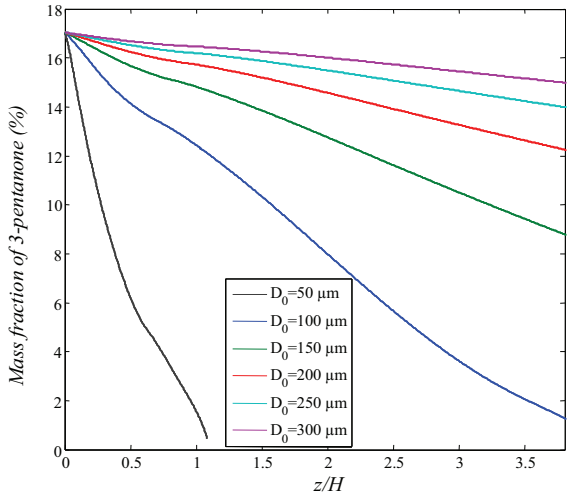

Figure 10. Computed 3-pentanone mass-fractions (Y_{3P}) evolution as a function of the downstream position for different initial droplet diameter.

The comparison between the measured and computed 3-pentanone liquid and gas flow-rate is displayed in figure 11. On the one hand, the calculated 3-pentanone liquid flow-rate tends quickly to overestimate the measured values using LIF. On the other hand, the comparison between the calculated 3-pentanone flow-rate in the gas phase is in correct agreement with the measured values from z/H=3.

One of the potential explanations could be linked to the fact that the effect of turbulence is not taken into account: turbulence tends to increase the vaporization rate due to longer residence time of the droplets in the evaporation chamber, caused by stochastic trajectories of the droplets. On the other hand, turbulence can lead to the formation of clusters of droplets, which tends to reduce the evaporation. These phenomena are, in this case, probably not dominant, since the calculations for the vapour of 3-pentanone seems in correct agreement with the experimental data. Also, the numerical simulation does not account for the droplet collisions onto the channel walls, which may reduce the number of liquid droplets crossing really a cross-section.

The second explanation could be found in the PLIF measurement technique. Generally, the LIF signal incoming from a droplet is coarsely proportional to the droplet volume (i.e. proportional to D^3). If the CCD camera dynamic is tuned on the intensity emitted by the biggest droplets (i.e. $D_{\max} \approx 270\ \mu m$), corresponding then to 65536 grey levels, the smallest detected droplet diameter (D_{min}) would be given by :

$$D_{\min} = D_{\max}\left(\frac{I_{\min}}{65536}\right)^{1/3}$$

where I_{min} is the minimum intensity detected by the CCD camera due to the threshold and the different image processing applied to discriminate the liquid droplets. The total dynamic range in term of detected intensity is estimated at 40, when all the image processing steps are considered. With $D_{\max} \approx 270\ \mu m$, the minimum detected diameter would be $D_{\min} \approx 80\ \mu m$. Consequently, if all the droplets smaller than D_{min} are ignored by the PLIF measurements and because droplet diameters tends to reduce due to evaporation, it appears clearly that the measured evaporation can be easily overestimated, leading to a smaller measured liquid 3-pentanone flowrate.
A correction coefficient α_{signal} can be applied to correct the signal from the detection dynamic range effect:

$$\alpha_{signal} = \int_{D_{\min}}^{+\infty} \rho_l \frac{\pi D^3}{6} Y_{3-p}(D) P(D) dD \Big/ \int_0^{+\infty} \rho_l \frac{\pi D^3}{6} Y_{3-p}(D) P(D) dD$$

A third explanation can be found in the mechanism of fluorescence emission of a liquid droplet seeded with a fraction of 3-pentanone. Due to the strong concentration of 3-pentanone in the droplets, the collected fluorescence signal is strongly affected by the absorption of the incident laser radiation at 266 nm. This phenomenon was described in details by Maqua et al. [13], in the case of ethanol droplets seeded with acetone. According to Maqua et al. [13], the fluorescence S_d emitted by a droplet can be written as:

$$S_d = K I_0 C_{l,3-p} D^3 \xi\left(C_{l,3-p}, D\right)$$

where K is constant, I_0 is the incident laser intensity, $C_{l,3-p}$ is the 3-pentanone molar concentration and $\xi\left(C_{l,3-p}, D\right)$ is the excitation efficiency of the droplet, taking into account the absorption of the incident laser beam:

$$\xi\left(C_{l,3-p}, D\right) = \int_V I_l\left(\vec{x}, C_{l,3-p}\right) dV \Big/ \int_V I_l\left(\vec{x}, C_{l,3-p} = 0\right) dV$$

where V is the droplet volume and I_l is the local laser excitation intensity at each $\vec{x}$ positions.
According to Ritchie and Seitzman [14], the efficiency can be simplified as:

$$\xi\left(C_{l,3-p}, D\right) \approx e^{-\varepsilon_{3-p} C_{l,3-p} D^{1.1}}$$

where ε_{3-p} is the molar extinction coefficient of the liquid 3-pentanone. The further calculations were performed with the value of ε_{3-p} corresponding to liquid acetone given by Maqua et al. [13], in absence of reliable value for liquid 3-pentanone.
The excitation efficiency factor is represented in figure 12 as a function of the 3-pentanone mass-fraction, for different droplet diameters. This efficiency decreases as the droplet diameter and 3-pentanone mass-fraction increases.
According to equations and , the liquid 3-pentanone mass flow-rate can be corrected by a coefficient α_{abs} taking into account the signal extinction within the droplets due to absorption:

$$\alpha_{abs} = \int_0^{+\infty} K C_{l,3-p} D^3 \xi\left(C_{l,3-p}, D\right) P(D) dD \Big/ \int_0^{+\infty} K C_{l,3-p} D^3 P(D) dD$$

Both correction coefficients α_{signal} and α_{abs} can be calculated at all the axial positions and can be used to correct the initial condition at z/H=0.6 (Eq.) and the calculated values of the liquid 3-pentanone flowrate at all the considered downstream positions.

The corrected values are also reported in figure 11. The most relevant correction is linked to absorption phenomena. The correction operated on the detection dynamic range has a moderate importance (on the order of a 3%), because mainly the smallest droplets, carrying a small mass of 3-pentanone, are affected. The initial evaporation appear much lower than for the uncorrected values, between z/H=0 and z/H=0.6, due to the presence of big droplets in this area, which are much more affected by absorption phenomena. The importance of this phenomenon tends to decrease for farther downstream positions as the droplet sizes decrease due to evaporation. However, despite of the applied corrections, the measured depletion of the 3-pentanone liquid flowrate remains slightly higher than the one predicted by the calculation. The agreement between the measurements performed in the gas phase and the calculations remains correct.

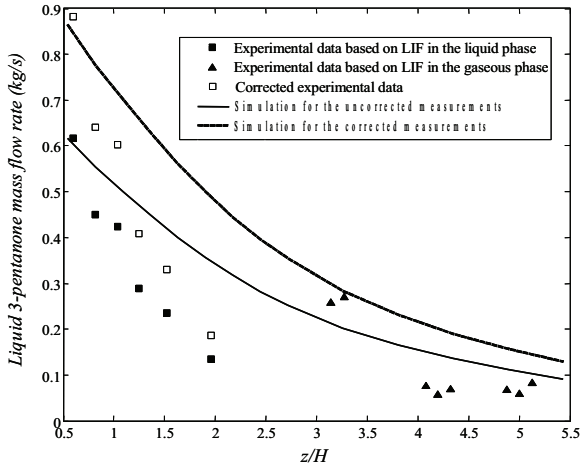

Figure 11. Liquid and 3-pentanone flow-rate: comparison between experimental (non-corrected and corrected) and numerical values.

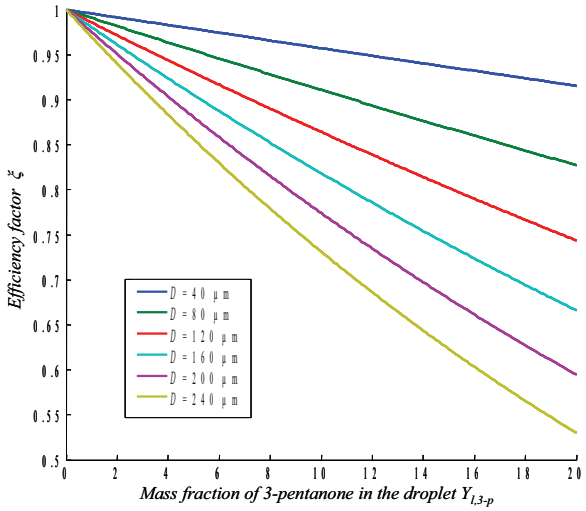

Figure 12. Evolution of the excitation efficiency factor of the droplet as a function of the 3-pentanone mass-fraction and initial droplet diameter.

Conclusions

PLIF measurements of liquid and gas concentrations of 3-pentanone have been performed in a turbulent over-heated channel flow, where a spray made of a binary mixture of n-octane and 3-pentanone was injected.
Post-processing of the experimental data took into account:
- the combined effects of the PLIF sensitivity to droplet volume and the dynamic of the fluorescence signal detection range,
- the extinction of the incident laser radiation in the liquid droplets.

A simple numerical simulation based on the isolated droplet model and discrete component approach shows a reasonable agreement between the data obtained on the gas phase and the calculations as the agreement remains not satisfactory on the liquid phase even after corrections of the experimental data.

Nomenclature

a	Thermal diffusivity [$m^2.s^{-1}$]
C	Molar concentration [$mol.l^{-1}$]
C_p	Specific heat capacity [$J.kg.K^{-1}$]
D	Droplet diameter [m]
ρ	Density [$kg \cdot m^{-3}$]
L_v	Latent heat of vaporization [$J.kg^{-1}$]
λ	Thermal conductivity [$J.K^{-1}.m^{-1}$]
$\dot{m}$	Mass flowrate [$kg.s^{-1}$]
μ	Dynamic viscosity [$Pa.s^{-1}$]
$P(X)$	Probability of X
Pr	Prandtl number
Re	Reynolds number
V_d	Droplet velocity [$m.s^{-1}$]
x	Axial coordinate [m]

y	Radial coordinate [m]
Y	Mass fraction

Subscripts

g	gas
l	liquid

References

[1] Birouk M., Gökalp I., *Progress in Energy and Combustion Science* 32: 408-423 (2006).
[2] Birouk, M., Chauveau C., Sarh B., Quilgars A., Gokalp I., *Combustion Science and Technology* 113(1): 413-428 (1996).
[3] Sornek R. J., R. Dobashi, T. Hirano, *Combustion and Flame* 120(4) : 479–491 (2000).
[4] Sirignano W., *Fluid Dynamics and Transport of Droplets and Sprays*, Cambridge University Press (1999).
[5] Abramzon B., Sirignano W.A., *Int. J. Heat Mass Transfer* 32 : 1605-1618 (1989).
[6] Videto B.D., Santavicca B.A. , *Combustion Science and technology* 76: 159-164 (1991).
[7] Cochet M., Bazile R., Ferret B., Cazin S., *Experiments In Fluids* 47(3), 379–394 (2009).
[8] Koch, J. and Hanson R., *Applied Physics B* 76, 319-324 (2003).
[9] Modica V., Guibert P., *Applied Physics B* 87: 193-204 (2007).
[10] Orain M., Grisch F., Rossow B., *Congrès Francophone de Techniques Laser, CFTL 2008*, Futuroscope, Poitiers, 16-19 septembre (2008).
[11] Moreau F., *PhD. Thesis*, Institut National Polytechnique de Toulouse - Université de Toulouse (2010).
[12] Tong A. Y., Sirignano WA., *Combustion and Flame* 66 : 221-235 (1986).
[13] Maqua C., Deprédurand V., Castanet G., Wolff M., Lemoine F., *Experiments in Fluids* 43 : 979-992 (2007).
[14] Ritchie B.D., Seitzman J.M. (2001), *AIAA paper* 2001-0414 (2001).